

Inelastic effects in molecular junctions in the Coulomb and Kondo regimes: Nonequilibrium equation-of-motion approach

Michael Galperin,¹ Abraham Nitzan,² and Mark A. Ratner¹

¹*Department of Chemistry and Nanotechnology Center, Northwestern University, Evanston, Illinois 60208, USA*

²*School of Chemistry, The Sackler Faculty of Science, Tel Aviv University, Tel Aviv 69978, Israel*

(Received 20 February 2007; revised manuscript received 23 April 2007; published 2 July 2007)

Inelastic effects in the Coulomb blockade and Kondo regimes of electron transport through molecular junctions are considered within a simple nonequilibrium equation-of-motion (EOM) approach. The scheme is self-consistent and can qualitatively reproduce the main experimental observations of vibrational features in the Coulomb blockade [H. Park *et al.*, *Nature (London)* **407**, 57 (2000)] and Kondo [L. H. Yu *et al.*, *Phys. Rev. Lett.* **93**, 266802 (2004)] regimes. Considerations similar to the equilibrium EOM approach by Meir *et al.* [Phys. Rev. Lett. **66**, 3048 (1991); **70**, 2601 (1993)] are used on the Keldysh contour to account for the nonequilibrium nature of the junction, and dressing by appropriate Franck-Condon factors is used to account for vibrational features. Results of the equilibrium EOM scheme by Meir *et al.* are reproduced in the appropriate limit.

DOI: [10.1103/PhysRevB.76.035301](https://doi.org/10.1103/PhysRevB.76.035301)

PACS number(s): 73.23.Hk, 72.10.Di, 73.63.-b, 85.65.+h

I. INTRODUCTION

Fast development of experimental techniques in the area of molecular electronics makes it possible to observe the response of molecular conduction junctions in a wide range of external parameters, such as source-drain and gate voltages.¹ Coulomb blockade (that characterizes the weak molecule-lead coupling limit), where transport through the molecular junction is suppressed due to high charging energy, and Kondo effect (encountered at sufficiently low temperature and strong molecule-lead coupling), when a correlation between localized (molecular) and band (contacts) electrons manifests itself in molecular junctions as a maximum in electrical conductance near $V_{sd} \sim 0$, were observed in the I/V_{sd} characteristics of such junctions.²⁻⁷ These are often accompanied by vibrational features that result from coupling between electronic and vibrational degrees of freedom. The latter can be associated with molecular center-of-mass motion⁸ or with intramolecular vibrations.^{2,4,6}

Early theoretical approaches to transport in the Coulomb blockade regime were either based on linear-response theory for near-equilibrium situations⁹⁻¹³ or by treating transport at the level of quasiclassical rate equations.^{14,15} While the second approach to nonequilibrium transport is justified in the case of pure Coulomb blockade (where hopping between molecule and contacts is rare), the intermediate regime, e.g., the case of stronger molecule-lead coupling relevant for observation of nonequilibrium Kondo resonance, should be treated at a more sophisticated level. Recent approaches dealing with nonequilibrium Coulomb blockade and/or Kondo effect are based on either the slave-boson technique,¹⁶⁻¹⁹ the equation-of-motion method,^{18,20-22} the Fock-space rate equation scheme,¹⁵ or the contour perturbation theory.^{11,23-29} Inelastic effects were not considered in the references above.

Here, we present a simple generalization of the equilibrium equation-of-motion approach used in the Coulomb^{10,30} regime (also later applied to the Kondo³¹ situation) to the case of nonequilibrium transport. The main difference be-

tween our approach and earlier nonequilibrium EOM studies^{18,21,22} is the simple appealing structure of the Green function, the evaluation of which (in the absence of electron-phonon coupling) does not require a time-consuming self-consistent procedure. As was indicated earlier,³⁰ this Green function expression reduces to the exact solution both for an isolated molecule and in the limit of noninteracting electrons. We also generalize this basic scheme to include inelastic effects approximately, within an approach based on the Born-Oppenheimer approximation that is commonly used in the Marcus theory of electron transfer.³² Numerical calculations are performed and qualitative correspondence to experimental data is demonstrated.

Our model and theoretical procedure are presented in Sec. II. Numerical results for the Coulomb blockade regime are given and discussed in Sec. III. The Kondo regime is discussed in Sec. IV. Section V concludes.

II. MODEL AND METHOD

We describe the molecular junction within a single resonant level (molecular electronic orbital) model, with electron-electron on-site repulsion (Hubbard term) and polaronic coupling to a local vibrational mode. The latter is coupled to a bosonic thermal bath. The electronic orbital is coupled to two (L and R) free-electron reservoirs representing the leads, each at its own equilibrium.

The corresponding Hamiltonian is

$$\begin{aligned} \hat{H} = & \sum_{K=L,R} \sum_{k \in K, \sigma} \varepsilon_{k\sigma} \hat{c}_{k\sigma}^\dagger \hat{c}_{k\sigma} + \sum_{\sigma} \varepsilon_{\sigma} \hat{a}_{\sigma}^\dagger \hat{a}_{\sigma} + \omega_0 \hat{a}^\dagger \hat{a} \\ & + \sum_{\beta} \omega_{\beta} \hat{b}_{\beta}^\dagger \hat{b}_{\beta} + \sum_{K=L,R} \sum_{k \in K, \sigma} (V_{k\sigma} \hat{c}_{k\sigma}^\dagger \hat{a}_{\sigma} + \text{H.c.}) \\ & + U \hat{n}_{\uparrow} \hat{n}_{\downarrow} + M \hat{Q}_a \sum_{\sigma} \hat{n}_{\sigma} + \sum_{\beta} U_{\beta} \hat{Q}_a \hat{Q}_{\beta}, \end{aligned} \quad (1)$$

where $\sigma = \uparrow, \downarrow$ is the electron spin index, $\hat{c}_{k\sigma}$ ($\hat{c}_{k\sigma}^\dagger$) are destruction (creation) operators for electronic state $k\sigma$ in the

contacts, \hat{d}_σ (\hat{d}_σ^\dagger) destroys (creates) electron in the molecular orbital, \hat{a} (\hat{a}^\dagger) are second quantization operators for the local vibrational mode, and \hat{b}_β (\hat{b}_β^\dagger) are the corresponding boson operators for thermal bath modes. Also,

$$\hat{Q}_a = \hat{a} + \hat{a}^\dagger, \quad \hat{Q}_\beta = \hat{b}_\beta + \hat{b}_\beta^\dagger \quad (2)$$

are displacement operators for the corresponding modes and $\hat{n}_\sigma = \hat{d}_\sigma^\dagger \hat{d}_\sigma$. Here and below, we use $\hbar = 1$ and $e = 1$. After small polaron (canonical or Lang-Firsov) transformation,³³ the Hamiltonian takes the form (for details, see Ref. 34)

$$\begin{aligned} \hat{H} = & \sum_{K=L,R} \sum_{k \in K, \sigma} \varepsilon_{k\sigma} \hat{c}_{k\sigma}^\dagger \hat{c}_{k\sigma} + \sum_{\sigma} \bar{\varepsilon}_{\sigma} \hat{d}_{\sigma}^\dagger \hat{d}_{\sigma} + \omega_0 \hat{a}^\dagger \hat{a} + \sum_{\beta} \omega_{\beta} \hat{b}_{\beta}^\dagger \hat{b}_{\beta} \\ & + \sum_{K=L,R} \sum_{k \in K, \sigma} (\bar{V}_{k\sigma} \hat{c}_{k\sigma}^\dagger \hat{d}_{\sigma} + \text{H.c.}) + \bar{U} \hat{n}_{\uparrow} \hat{n}_{\downarrow} + \sum_{\beta} U_{\beta} \hat{Q}_a \hat{Q}_{\beta}, \end{aligned} \quad (3)$$

where

$$\bar{\varepsilon}_{\sigma} = \varepsilon_{\sigma} - M^2 / \omega_0, \quad (4)$$

$$\bar{U} = U - 2M^2 / \omega_0, \quad (5)$$

$$\bar{V}_{k\sigma} = V_{k\sigma} \hat{X}_a, \quad (6)$$

and where

$$\hat{X}_a = \exp(i\lambda_a \hat{P}_a), \quad \lambda_a = \frac{M}{\omega_0} \quad (7)$$

is the phonon shift generator operator with

$$\hat{P}_a = -i(\hat{a} - \hat{a}^\dagger). \quad (8)$$

\hat{P}_a [Eq. (8)] is the phonon momentum operator; we use the term phonon to characterize both molecular and bath vibrations.

The Hamiltonian in Eq. (3) is our starting point for the calculation of the steady-state current across the junction, using the nonequilibrium Green function (NEGF) expression derived in Refs. 30 and 35,

$$I_K = \frac{e}{\hbar} \sum_{\sigma} \int \frac{dE}{2\pi} [\Sigma_{K,\sigma}^{<}(E) G_{\sigma}^{>}(E) - \Sigma_{K,\sigma}^{>}(E) G_{\sigma}^{<}(E)]. \quad (9)$$

Here $\Sigma_{K,\sigma}^{(\cdot)}$ are lesser and greater projections of the self-energy due to coupling to the contact K ($K=L,R$),

$$\Sigma_{K,\sigma}^{<}(E) = i f_K(E) \Gamma_{K,\sigma}(E), \quad (10)$$

$$\Sigma_{K,\sigma}^{>}(E) = -i[1 - f_K(E)] \Gamma_{K,\sigma}(E), \quad (11)$$

with $f_K(E)$ the Fermi distribution in the contact K and

$$\Gamma_{K,\sigma}(E) = 2\pi \sum_{k \in K} |V_{k\sigma}|^2 \delta(E - \varepsilon_k). \quad (12)$$

The lesser and greater Green functions in Eq. (9) are Fourier transforms to energy space of projections onto the real time axis of the electron Green function on the Keldysh contour,

$$\begin{aligned} G_{\sigma}(\tau_1, \tau_2) &= -i \langle T_c \hat{d}_{\sigma}(\tau_1) \hat{d}_{\sigma}^{\dagger}(\tau_2) \rangle_H \\ &= -i \langle T_c \hat{d}_{\sigma}(\tau_1) \hat{X}_a(\tau_1) \hat{d}_{\sigma}^{\dagger}(\tau_2) \hat{X}_a^{\dagger}(\tau_2) \rangle_{\bar{H}}, \end{aligned} \quad (13)$$

where the subscripts H and \bar{H} indicate which Hamiltonian, Eq. (1) or (3), respectively, determines evolution of the system, and T_c is the contour ordering operator. In what follows, we use the second form and will drop the subscript \bar{H} while keeping in mind that time evolution is determined by the Hamiltonian in Eq. (3). We next decouple electron and phonon dynamics in the spirit of the Born-Oppenheimer theory within the Condon approximation,

$$G_{\sigma}(\tau_1, \tau_2) \approx G_{\sigma}^{(e)}(\tau_1, \tau_2) K(\tau_1, \tau_2), \quad (14)$$

where

$$G_{\sigma}^{(e)}(\tau_1, \tau_2) = -i \langle T_c \hat{d}_{\sigma}(\tau_1) \hat{d}_{\sigma}^{\dagger}(\tau_2) \rangle, \quad (15)$$

$$K(\tau_1, \tau_2) = \langle T_c \hat{X}_a(\tau_1) \hat{X}_a^{\dagger}(\tau_2) \rangle. \quad (16)$$

The shift generator correlation function K can be expressed within the second-order cumulant expansion in terms of the phonon Green function (for derivation, see Ref. 34),

$$K(\tau_1, \tau_2) = \exp\{\lambda_a^2 [iD_{P_a P_a}(\tau_1, \tau_2) - \langle \hat{P}_a^2 \rangle]\}, \quad (17)$$

$$D_{P_a P_a}(\tau_1, \tau_2) = -i \langle T_c \hat{P}_a(\tau_1) \hat{P}_a(\tau_2) \rangle, \quad (18)$$

while the phonon Green function D obeys approximately an equation which resembles the usual Dyson equation,

$$\begin{aligned} D_{P_a P_a}(\tau, \tau') &= D_{P_a P_a}^{(0)}(\tau, \tau') + \int_c d\tau_1 \int_c d\tau_2 D_{P_a P_a}^{(0)}(\tau, \tau_1) \\ &\quad \times \Pi_{P_a P_a}(\tau_1, \tau_2) D_{P_a P_a}(\tau_2, \tau'), \end{aligned} \quad (19)$$

with

$$\begin{aligned} \Pi_{P_a P_a}(\tau_1, \tau_2) &= \sum_{\beta} |U_{\beta}|^2 D_{P_{\beta} P_{\beta}}(\tau_1, \tau_2) \\ &\quad - i\lambda_a^2 \sum_{k \in \{L,R\}, \sigma} |V_{k\sigma}|^2 [g_{k,\sigma}(\tau_2, \tau_1) \\ &\quad \times G_{\sigma}^{(e)}(\tau_1, \tau_2) K(\tau_1, \tau_2) + (\tau_1 \leftrightarrow \tau_2)] \end{aligned} \quad (20)$$

the analog of a self-energy. $g_{k,\sigma}$ is the free-electron GF in the contact, defined in Eq. (31) below.

To obtain an expression for the Green function $G_{\sigma}^{(e)}$, we follow the equation-of-motion (EOM) method of Meir *et al.*^{10,30} where it was applied for a near-equilibrium situation, except that we consider the EOMs on the Keldysh contour in order to take into account the nonequilibrium condition. In the spirit of the Born-Oppenheimer approximation, we regard the shift generator operators \hat{X}_a as parameters incorporated into transfer-matrix elements $\bar{V}_{k\sigma}$. The solution of the electronic problem is thus carried out as in the absence of electron-phonon coupling^{10,30} with renormalized parameters U ($\rightarrow \bar{U}$) and V ($\rightarrow \bar{V}$). The result is then averaged over the phonon subspace. This average is obviously not needed in

the absence of electron-phonon coupling, $M=0$, in which case $G_\sigma = G_\sigma^{(e)}$. This leads to (for derivation, see Appendix A)

$$G_\sigma^{(e)}(\tau_1, \tau_2) = [1 - \langle \hat{n}_{\bar{\sigma}} \rangle] G_{2,\sigma}^{(e)}(\tau_1, \tau_2) + \langle \hat{n}_{\bar{\sigma}} \rangle G_{3,\sigma}^{(e)}(\tau_1, \tau_2), \quad (21)$$

where the GFs $G_{i,\sigma}^{(e)}$ ($i=\{1,2,3,4\}$) obey

$$\int_c d\tau \hat{G}_{i,\sigma}^{-1}(\tau_1, \tau) G_{i,\sigma}^{(e)}(\tau, \tau_2) = \delta(\tau_1, \tau_2), \quad (22)$$

with

$$\hat{G}_{1,\sigma}^{-1}(\tau, \tau') = \left[\delta(\tau, \tau') \left(i \frac{\partial}{\partial \tau} - \varepsilon_\sigma - U \right) - \Sigma_{\sigma 0}(\tau, \tau') - \Sigma_{\sigma 3}(\tau, \tau') \right], \quad (23)$$

$$\hat{G}_{2,\sigma}^{-1}(\tau, \tau') = \left[\delta(\tau, \tau') \left(i \frac{\partial}{\partial \tau} - \varepsilon_\sigma \right) - \Sigma_{\sigma 0}(\tau, \tau') + U \int_c d\tau'' G_{1,\sigma}^{(e)}(\tau, \tau'') \Sigma_{\sigma 1}(\tau'', \tau') \right], \quad (24)$$

$$\hat{G}_{3,\sigma}^{-1}(\tau, \tau') = \left[\delta(\tau, \tau') \left(i \frac{\partial}{\partial \tau} - \varepsilon_\sigma - U \right) - \Sigma_{\sigma 0}(\tau, \tau') - U \int_c d\tau'' G_{4,\sigma}^{(e)}(\tau, \tau'') \Sigma_{\sigma 2}(\tau'', \tau') \right], \quad (25)$$

$$\hat{G}_{4,\sigma}^{-1}(\tau, \tau') = \left[\delta(\tau, \tau') \left(i \frac{\partial}{\partial \tau} - \varepsilon_\sigma \right) - \Sigma_{\sigma 0}(\tau, \tau') - \Sigma_{\sigma 3}(\tau, \tau') \right]. \quad (26)$$

Expressions for ‘‘self-energies’’ $\Sigma_{\sigma i}$ ($i=\{0,1,2,3\}$) are given by

$$\Sigma_{\sigma 0}(\tau, \tau') = \sum_k |V_{k\bar{\sigma}}|^2 g_{k,\sigma}(\tau, \tau') \langle T_c \hat{X}_a^\dagger(\tau) \hat{X}_a(\tau') \rangle, \quad (27)$$

$$\Sigma_{\sigma 1}(\tau, \tau') = \sum_k \langle \hat{n}_{k\bar{\sigma}} \rangle [|V_{k\bar{\sigma}}|^2 g_{k,\bar{\sigma}}^{(1)}(\tau, \tau') \langle T_c \hat{X}_a^\dagger(\tau) \hat{X}_a^\dagger(\tau') \rangle + |V_{k\bar{\sigma}}|^2 g_{k,\bar{\sigma}}^{(2)}(\tau, \tau') \langle T_c \hat{X}_a^\dagger(\tau) \hat{X}_a(\tau') \rangle], \quad (28)$$

$$\Sigma_{\sigma 2}(\tau, \tau') = \Sigma_{\sigma 3}(\tau, \tau') - \Sigma_{\sigma 1}(\tau, \tau'), \quad (29)$$

$$\Sigma_{\sigma 3}(\tau, \tau') = \sum_k [|V_{k\bar{\sigma}}|^2 g_{k,\bar{\sigma}}^{(1)}(\tau, \tau') \langle T_c \hat{X}_a(\tau) \hat{X}_a^\dagger(\tau') \rangle + |V_{k\bar{\sigma}}|^2 g_{k,\bar{\sigma}}^{(2)}(\tau, \tau') \langle T_c \hat{X}_a^\dagger(\tau) \hat{X}_a(\tau') \rangle], \quad (30)$$

with $\bar{\sigma}$ denoting the spin opposite to σ . The free-electron propagators $g_{k,\sigma}$ and $g_{k,\bar{\sigma}}^{(j)}$, $j=1,2$ are defined by

$$\left(i \frac{\partial}{\partial \tau} - \varepsilon_{k\sigma} \right) g_{k,\sigma}(\tau, \tau') = \delta(\tau, \tau'), \quad (31)$$

$$\left(i \frac{\partial}{\partial \tau} + \varepsilon_{k\bar{\sigma}} - \varepsilon_\sigma - \varepsilon_{\bar{\sigma}} - U \right) g_{k,\bar{\sigma}}^{(1)}(\tau, \tau') = \delta(\tau, \tau'), \quad (32)$$

$$\left(i \frac{\partial}{\partial \tau} - \varepsilon_{k\bar{\sigma}} - \varepsilon_\sigma + \varepsilon_{\bar{\sigma}} \right) g_{k,\bar{\sigma}}^{(2)}(\tau, \tau') = \delta(\tau, \tau'). \quad (33)$$

For $M=0$, \bar{V} Franck-Condon (FC) factors (i.e., shift generator correlation functions $\langle XX^\dagger \rangle$ and $\langle X^\dagger X \rangle$) should be taken as 1 in Eqs. (27)–(30). Below the SEs in this case will be denoted $\Sigma_{\sigma j}^{(e)}$ ($j=0,1,2,3$). Note that the retarded projections of these are equivalent to the SEs introduced in Ref. 10. For example, taking the retarded projection of Eq. (30) and Fourier transforming to energy space leads to

$$\Sigma_{\sigma 3}^{(e)r}(E) = \sum_{k \in L,R} |V_{k\bar{\sigma}}|^2 \left(\frac{1}{E + \varepsilon_{k\bar{\sigma}} - \varepsilon_\sigma - \varepsilon_{\bar{\sigma}} - U} + \frac{1}{E - \varepsilon_{k\bar{\sigma}} - \varepsilon_\sigma + \varepsilon_{\bar{\sigma}}} \right), \quad (34)$$

which is identical to Eq. (9) in Ref. 10 for $i=3$. Other expressions are obtained in a similar way.

Consider first the case with no electron-phonon coupling. The structure of expression (21) for the nonequilibrium GF $G_\sigma^{(e)}$ is appealingly simple and has two important implications. First, it provides a convenient way for handling the Hubbard repulsion term U . While the case of weak electron-electron interaction can be handled by taking this term as a perturbation,²⁶ the case of strong interaction cannot be handled in this way, but including U in H_0 makes standard diagrammatic techniques unusable.³⁶ This difficulty is circumvented by Eq. (21), which expresses the system GF as a superposition (with the level population n defining weight parameters) of simpler GFs associated with Hamiltonians that do not depend on U (apart from a parametric energy shift) for which Wick’s theorem is applicable. Secondly, by using the EOM method on the Keldysh contour, we are able to derive not only the retarded GF as in Ref. 10 but also the other projections, in particular, the lesser GF that can be used to evaluate the level populations,

$$\langle \hat{n}_\sigma \rangle = -i/2\pi \int dE G_\sigma^{(e)<}(E). \quad (35)$$

This, together with Eq. (21), leads to an explicit expression for $\langle \hat{n}_\sigma \rangle$. Denoting

$$I_{i,\sigma} = -i/2\pi \int dE G_{i,\sigma}^{(e)<}(E), \quad (36)$$

one gets from Eq. (21)

$$\langle \hat{n}_\sigma \rangle = (1 - \langle \hat{n}_{\bar{\sigma}} \rangle) I_{2,\sigma} + \langle \hat{n}_{\bar{\sigma}} \rangle I_{3,\sigma}, \quad (37)$$

and hence

$$\langle \hat{n}_\sigma \rangle = \frac{I_{2,\sigma} - I_{2,\bar{\sigma}}(I_{2,\sigma} - I_{3,\sigma})}{1 - (I_{2,\bar{\sigma}} - I_{3,\bar{\sigma}})(I_{2,\sigma} - I_{3,\sigma})}. \quad (38)$$

$G_{i,\sigma}^{(e)<}$ can be calculated from the Keldysh equation,

$$G_{i,\sigma}^{(e)<}(E) = G_{i,\sigma}^{(e)r}(E)\Sigma_{i,\sigma}^{(e)<}(E)G_{i,\sigma}^{(e)a}(E), \quad (39)$$

with $\Sigma_{i,\sigma}^{(e)<}$ ($i=1,2,3,4$) being lesser projections of the corresponding self-energies presented in Eqs. (23)–(26), i.e.,

$$\Sigma_{1,\sigma}^{(e)}(\tau, \tau') = \Sigma_{\sigma 0}(\tau, \tau') + \Sigma_{\sigma 3}(\tau, \tau'), \quad (40)$$

$$\Sigma_{2,\sigma}^{(e)}(\tau, \tau') = \Sigma_{\sigma 0}(\tau, \tau') - U \int_c d\tau'' G_{1,\sigma}^{(e)}(\tau, \tau'')\Sigma_{\sigma 1}(\tau'', \tau'), \quad (41)$$

$$\Sigma_{3,\sigma}^{(e)}(\tau, \tau') = \Sigma_{\sigma 0}(\tau, \tau') + U \int_c d\tau'' G_{4,\sigma}^{(e)}(\tau, \tau'')\Sigma_{\sigma 2}(\tau'', \tau'), \quad (42)$$

$$\Sigma_{4,\sigma}^{(e)}(\tau, \tau') = \Sigma_{\sigma 0}(\tau, \tau') + \Sigma_{\sigma 3}(\tau, \tau'), \quad (43)$$

and expressions for $\Sigma_{\sigma i}$ ($i=\{0,1,2,3\}$) given by Eqs. (27)–(30).

Since $G_{i,\sigma}^{(e)<}$ ($i=1,2,3,4$), and therefore $I_{i,\sigma}$ do not depend on $\langle \hat{n}_\sigma \rangle$, Eq. (38) is an explicit expression for $\langle \hat{n}_\sigma \rangle$ and not, as might have expected, an equation that needs to be solved self-consistently. Equation (21) therefore constitutes an explicit expression for $G_\sigma^{(e)}$ that can be evaluated directly once the $G_{i,\sigma}^{(e)<}$ are known. Thus, the Keldysh contour based consideration provides full information on the nonequilibrium system, and no separate considerations (as noncrossing approximation used in Ref. 32) are needed in order to estimate the level population. Note that both Ref. 32 and our consideration give only qualitative description of the Kondo effect, since correlation between localized spin at the level and opposite spin cloud in the contacts is treated perturbatively.

When electron-phonon interaction is present, Eq. (35) remains valid. This results from the fact that $K^<(t,t)=1$, so that $G_\sigma^<(t,t)=G_\sigma^{(e)<}(t,t)$; still, one has to deal with a self-consistent procedure. Indeed, the phonon GF $D_{P_a P_a}$ [and hence shift generator correlation function K , see Eq. (17)] depends on the electronic GF $G_\sigma^{(e)}$ through its self-energy $\Pi_{P_a P_a}$, Eq. (20). On the other hand, the electron GF $G_\sigma^{(e)}$ depends on the shift generator correlation function K through its self-energies $\Sigma_{\sigma i}$ ($i=\{0,1,2,3\}$), Eqs. (27)–(30). The resulting procedure is described in detail in Ref. 34. The only difference that enters here is the need to obtain the different self-energies defined in Eqs. (27)–(30).

As discussed in Ref. 34, the calculations involving electron-phonon interaction, when multiplication by the FC factor is necessary, are facilitated by repeatedly moving between the time and energy domains. This is done using fast Fourier transform. In the calculations, we use (following Ref. 17) for the retarded projection of $\Sigma_{K,\sigma 0}$,

$$\Sigma_{K,\sigma 0}^{(e)r}(E) = \frac{1}{2} \frac{\Gamma_{K,\sigma}^{(0)} W_{K,\sigma}^{(0)}}{E - E_{K,\sigma}^{(0)} + iW_{K,\sigma}^{(0)}}, \quad (44)$$

while its lesser projection is given by Eq. (10), where

$$\Gamma_{K,\sigma 0}(E) = -2 \text{Im}[\Sigma_{K,\sigma 0}^{(e)r}(E)]. \quad (45)$$

We take $W_{K,\sigma}^{(0)}=10U$ and $E_{K,\sigma}^{(0)}$ taken at the Fermi level, defined to be the zero of energy ($E_F=0$). This form will ensure convergence of the integrals. A bandwidth ten times the Coulomb repulsion is enough to get essentially constant density of contact states in the relevant energy region (wide band). $\Gamma_{K,\sigma}^{(0)}$ is taken to be much smaller than U to simulate the Coulomb blockade regime; exact numbers are indicated in the calculation parameters below.

The biased junction was characterized by the choice

$$\mu_L = E_F + \eta e V_{sd}, \quad \mu_R = E_F - (1 - \eta)e V_{sd}, \quad (46)$$

with voltage division factor $\eta=0.5$. In calculations with $M \neq 0$, where an iterative procedure was used, convergence was assumed when population differences (electronic population for both spins and vibrational population) between consecutive iteration steps were less than the predefined tolerance, taken to be 10^{-4} . The application of a gate potential was represented by taking

$$\bar{\epsilon}_\sigma(V_g) = \bar{\epsilon}_\sigma(V_g = 0) + eV_g. \quad (47)$$

Note that V_g in Eq. (47) is the effective potential at the molecule, which is usually considerably smaller than the bare potential applied to the gate.

In what follows, we apply the procedure outlined above in two situations. In Sec. III, we focus on Coulomb blockade phenomena. In Sec. IV, we describe the application to Kondo physics by keeping the temperature low enough and by assigning finite lifetimes to the metal electrons.

III. NUMERICAL RESULTS IN THE COULOMB BLOCKADE REGIME

When dealing with the Coulomb-blockade-type calculations, the electronic part (without the FC factors) of the lesser and greater projections of $\Sigma_{\sigma j}$ ($j=1,2,3$) are obtained from Eqs. (28)–(30) and given by

$$\Sigma_{\sigma 1}^{(e)<}(E) = i \sum_{K=L,R} [\Gamma_{K,\bar{\sigma}}(E_{1\sigma})f_K^2(E_{1\sigma}) + \Gamma_{K,\bar{\sigma}}(E_{2\sigma})f_K^2(E_{2\sigma})], \quad (48)$$

$$\begin{aligned} \Sigma_{\sigma 1}^{(e)>}(E) = & -i \sum_{K=L,R} \{ \Gamma_{K,\bar{\sigma}}(E_{1\sigma})f_K(E_{1\sigma})[1 - f_K(E_{1\sigma})] \\ & + \Gamma_{K,\bar{\sigma}}(E_{2\sigma})f_K(E_{2\sigma})[1 - f_K(E_{2\sigma})] \}, \end{aligned} \quad (49)$$

$$\Sigma_{\sigma 2}^{(e)>,<}(E) = \Sigma_{\sigma 3}^{(e)>,<}(E) - \Sigma_{\sigma 1}^{(e)>,<}(E), \quad (50)$$

$$\Sigma_{\sigma 3}^{(e)<}(E) = i \sum_{K=L,R} [\Gamma_{K,\bar{\sigma}}(E_{1\sigma})f_K(E_{1\sigma}) + \Gamma_{K,\bar{\sigma}}(E_{2\sigma})f_K(E_{2\sigma})], \quad (51)$$

$$\begin{aligned} \Sigma_{\sigma 3}^{(e)>}(E) = & -i \sum_{K=L,R} \{ \Gamma_{K,\bar{\sigma}}(E_{1\sigma})[1 - f_K(E_{1\sigma})] \\ & + \Gamma_{K,\bar{\sigma}}(E_{2\sigma})[1 - f_K(E_{2\sigma})] \}, \end{aligned} \quad (52)$$

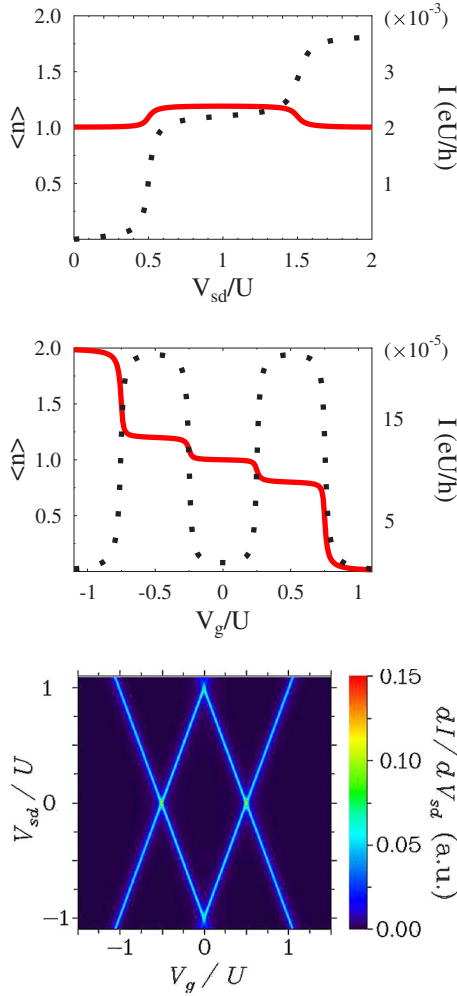


FIG. 1. (Color online) Elastic resonant tunneling. Average population (solid line, left axis) and current (dotted line, right axis) as function of (a) V_{sd} at fixed $V_g = -U/4$ and (b) V_g at fixed $V_{sd} = U/2$. (c) Contour plot of dI/dV_{sd} vs V_g and V_{sd} . See text for parameters. Note that V_{sd} axis range in (a) goes beyond that in (c).

where $E_{1\sigma} = \bar{\epsilon}_\sigma + \bar{\epsilon}_{\bar{\sigma}} + U - E$ and $E_{2\sigma} = E - \bar{\epsilon}_\sigma + \bar{\epsilon}_{\bar{\sigma}}$. Retarded projection of the full SEs (after dressing by FC factors) are obtained using Lehmann representation.³³

Consider first the situation where no electron-phonon coupling is present, $M=0$. Figure 1(c) shows a conductance contour plot as a function of the gate and source-drain voltages for a system characterized by $\epsilon_\sigma = -0.5$, $\Gamma_{K,\sigma}^{(0)} = 0.01$, and $T = 10^{-4}$ (all parameters are in units of U). Figure 1(a) presents average level population (solid line) and current (dotted line) plotted as a function of V_{sd} at fixed $V_g = -U/4$. I/V_{sd} curve shows two Coulomb addition plateaus, as is expected for a doubly degenerate single level. Figure 1(b) is a similar graph as a function of V_g at fixed $V_{sd} = U/2$. The usual Coulomb blockade diamond structure is observed in the bottom graph. Naturally, at high positive V_g , the level is unpopulated, while at high negative V_g , it is fully populated ($\langle \hat{n} \rangle = 2$). Within the conduction diamond, the average population is 1, indicating the Coulomb blockade situation. Intermediate regions provide fractional average populations due to partial occupation of the levels.

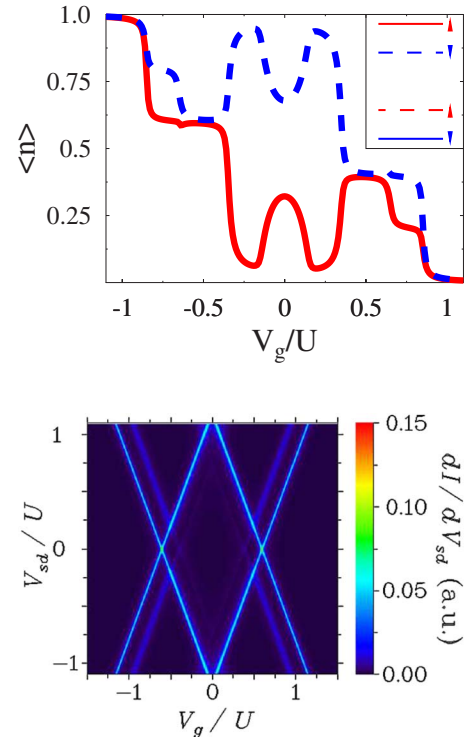


FIG. 2. (Color online) Elastic resonant tunneling under applied magnetic field. Average populations of spin-up (solid line) and spin-down (dashed line) levels vs V_g at fixed $V_{sd} = U/2$ (top). Contour plot of dI/dV_{sd} (bottom) vs V_g and V_{sd} . Inset shows two possible states (solid and dashed lines) of the molecule. See text for parameters.

The case $\epsilon_\sigma \neq \epsilon_{\bar{\sigma}}$, which may correspond to magnetic-field removal of spin degeneracy, is shown in Fig. 2. We take the split levels to be $\epsilon_{\uparrow} = -0.6$ and $\epsilon_{\downarrow} = -0.4$, other parameters are identical to those of Fig. 1. This split results in splitting of the conductance lines, as is shown in the bottom graph. Note the different intensity of the lines outside the diamond, The difference becomes even more drastic inside the diamond. This result is in agreement with experimental observation.² The calculated average population of the two spin levels (top graph), where again the source-drain voltage is fixed at $V_{sd} = U/2$, shows their complex dependence on gate voltage. This behavior can be understood within a simple argument. The molecule in the junction can be in either of the two states sketched in the inset of the top graph by solid and dashed lines. The observed average is the sum of the two contributions with weights representing probability for the system to be in the state. A qualitative explanation is based on the assumption that the system strives to be in a minimum-energy situation (note that this explanation is only qualitative, since an energy minimum is not required in the nonequilibrium transport case, however, it might work to some extent in the blockade regime). Thus, the probability to be in the state indicated by solid lines in the inset is much higher than in the other. So, the most pronounced lines in conductance appear when chemical potentials cross the energy levels of this (solid line levels in the inset) state. Average population behavior can be explained with this consideration as well.

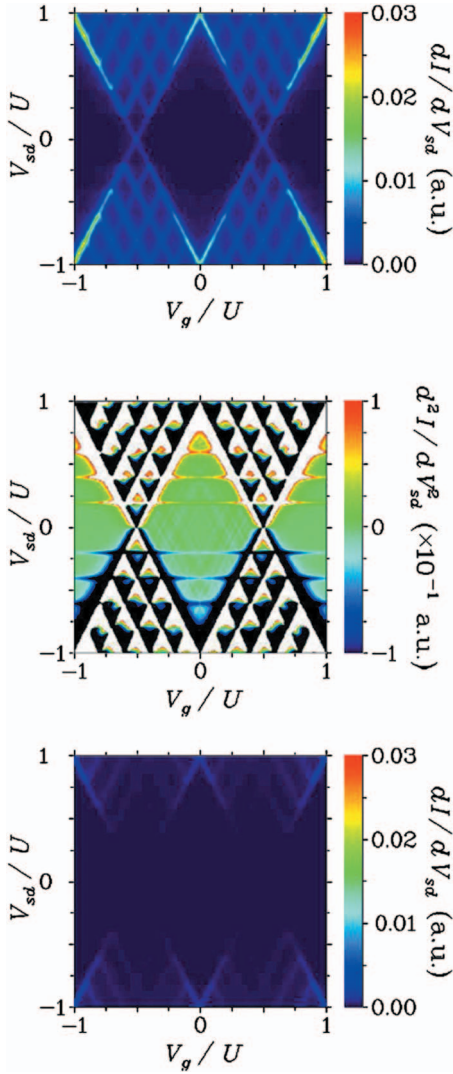


FIG. 3. (Color online) Inelastic tunneling. (a) Contour plot of dI/dV_{sd} vs V_g and V_{sd} . (b) Contour plot of d^2I/dV_{sd}^2 vs V_g and V_{sd} . White regions correspond to values outside the scale; (c) Franck-Condon blockade. See text for parameters.

In the presence of vibrational degrees of freedom, inelastic cotunneling (vibrational inelasticity) can be observed in conductance.^{6,7,37} The situation is illustrated within a zero-order calculation³⁸ using the parameters (in units of \bar{U}) $T = 10^{-3}$, $\bar{\varepsilon}_\sigma = -0.5$, $\Gamma_{K,\sigma}^{(0)} = 0.01$, $\omega_0 = 0.2$, and $M = 0.4$. The following points should be noted:

(1) Figure 3(a) shows the main Coulomb steps in the conductance map. In addition to elastic, vibrational sidebands corresponding to phonon creation by the tunneling electron are observed. Peaks corresponding to phonon absorption are not seen due to the low temperature employed in the calculation.

(2) Figure 3(b) represents the second derivative of current vs source-drain voltage map. In addition to resonant vibrational sidebands (lines along main Coulomb steps) observed in Fig. 3(a), here, one sees also inelastic electron tunneling spectroscopy (IETS) vibrational features (gate-voltage-

independent off-resonant vibrational features), as well as weak lines corresponding to phonon annihilation.

(3) The absence of vibrational sidebands or variable V_g for $V_{sd} < \omega_0$ is clearly seen from Fig. 3(a). This issue was first addressed in Ref. 39 and later confirmed by us.³⁴

(4) Suppression of the conduction signal at low source-drain voltage (the so-called Franck-Condon blockade⁴⁰) is seen from Fig. 3(a) as well. At even stronger electron-phonon coupling [Fig. 3(c); a zero-order calculation with the same parameters as in Fig. 3(a) except that $M = 0.6$], the low-voltage signal is suppressed completely.

(5) Note that while experimentally the scales in V_g and V_{sd} where Coulomb blockade diamonds are observed are very different (V_{sd} is of order of Coulomb repulsion energy, 100 mV, while V_g spans ~ 1 V), in our calculations, they are comparable. The reason for this is that experimentally, only part of the applied gate voltage affects the position of the molecular level relative to contact Fermi energy. This is due to two reasons: first, capacitance factors (charging of the junction) play a role, and second, gate voltage cannot be tuned to strongly affect the molecule because of small sizes of the junction.⁴¹ In our calculations, however, a rigid shift of molecular level is assumed.

IV. THE KONDO REGIME

The Kondo effect,⁴² a crossover from weak to strong coupling between localized (molecular) and band (contacts) electrons, manifests itself in molecular junctions as a maximum in electrical conductance near $V_{sd} \sim 0$ at low temperatures. Conduction in this regime was described by Meir *et al.*³¹ within an EOM scheme. The treatment has focused on the retarded GFs, making it necessary to get level populations from a separate calculation using the noncrossing approximation. In contrast, the NEGF EOM approach yields both the retarded and lesser GFs, and the needed level populations are obtained from the latter. This provides a single consistent theoretical framework that, as we show below, reproduces the results of Ref. 31. It should be noted, however, that this approach is still an approximation, since truncating the EOM hierarchy, Eqs. (A12)–(A17), implies neglect of correlations that may become important in the mixed valence situation when the level ε_σ (shifted by V_g) is close to the Fermi energy. Therefore, our nonequilibrium treatment of the Kondo regime is questionable beyond the low bias regime $E_F - \varepsilon_\sigma \gg eV_{sd}$, similar to the mean-field slave-boson approach^{19,42–44} where charge correlations are neglected by the mean-field approximation. In both approaches though, the needed correlations in spin fluctuations are maintained; in the present approach, this is done by keeping the correlation functions in Eqs. (A6)–(A8) as essential ingredients of the calculation.

Consider first the purely electronic case, $M = 0$. Following Ref. 31, we limit our consideration to the $U \rightarrow \infty$ limit. This leads to significant simplification while at the same time limiting the site to at most single occupancy, as required for observation of the Kondo effect.⁴⁵ From Eqs. (22)–(26), it follows that $G_{3,\sigma}^{(e)} \sim 1/U \rightarrow 0$ in this limit, while $G_{2,\sigma}^{(e)} \rightarrow G_{2,\sigma}^{(e,\infty)}$ satisfies the following Dyson equation:

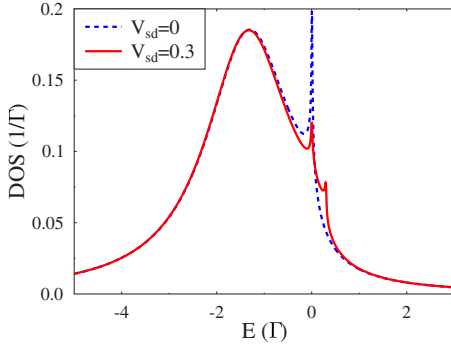


FIG. 4. (Color online) Bridge density of states in the Kondo regime for equilibrium (dashed line) and nonequilibrium (solid line) situations. See text for parameters.

$$\int_c d\tau \left[\left(i \frac{\partial}{\partial \tau} - \varepsilon_\sigma \right) \delta(\tau_1, \tau) - \Sigma_{\sigma 0}(\tau_1, \tau) - \Sigma_{\sigma 1}^{(\infty)}(\tau_1, \tau) \right] \times G_{2,\sigma}^{(e,\infty)}(\tau, \tau_2) = \delta(\tau_1, \tau_2), \quad (53)$$

with $\Sigma_{\sigma 0}$ defined in Eq. (27) and from Eq. (28) [because $g_{k,\bar{\sigma}}^{(1)} \rightarrow 0$ in the $U \rightarrow \infty$ limit; cf. Eq. (32)],

$$\Sigma_{\sigma 1}^{(\infty)}(\tau, \tau') = \sum_{K=L,R} \sum_{k \in K} |V_{k\bar{\sigma}}|^2 \langle \hat{n}_{k\bar{\sigma}} \rangle g_{k,\bar{\sigma}}^{(2)}(\tau, \tau'). \quad (54)$$

Thus from Eq. (21), it follows that the total GF in the $U \rightarrow \infty$ limit is

$$G_\sigma^{(e,\infty)} = (1 - \langle \hat{n}_{\bar{\sigma}} \rangle) G_{2,\sigma}^{(e,\infty)}(\tau_1, \tau_2). \quad (55)$$

The Kondo peak diverges unless the finite lifetime of metal electrons is taken into account. We incorporate this lifetime in the form introduced in Eq. (5) of Ref. 32 (which associates lifetime with scattering off the molecular state). Note that the Lorentzian form adopted following Ref. 17 for the coupling between molecule and contacts, Eq. (44), prevents ultraviolet divergence of integrals such as Eq. (B1) and allows analytic evaluation of $\Sigma_{\sigma 1}^{(\infty)}$ projections [see Appendix B, Eqs. (B10) and (B11)].

Equations (53)–(55) lead to the following form for the retarded projection of $G_\sigma^{(e,\infty)}$:

$$G_{2,\sigma}^{(e,\infty)r}(E) = \frac{1 - \langle \hat{n}_{\bar{\sigma}} \rangle}{E - \varepsilon_\sigma - \Sigma_{\sigma 0}(E) - \Sigma_{\sigma 1}^{(\infty)}(E)}, \quad (56)$$

where $\Sigma_{\sigma 0}(E)$ and $\Sigma_{\sigma 1}^{(\infty)}(E)$ are defined in Eqs. (44) and (B10), respectively. These expressions are identical to Eqs. (3) and (4) of Ref. 32. Note, however, that $\langle \hat{n}_{\bar{\sigma}} \rangle$ is now calculated from the lesser projection,

$$G_\sigma^{(e,\infty)<}(E) = (1 - \langle \hat{n}_{\bar{\sigma}} \rangle) G_{2,\sigma}^{(e,\infty)<}(E). \quad (57)$$

Figure 4 presents the bridge density of states in equilibrium (dashed line) and nonequilibrium (solid line) situations. Parameters of the calculation are (in units of $\Gamma_\sigma^{(0)} = \Gamma_{L,\sigma}^{(0)} + \Gamma_{R,\sigma}^{(0)}$) $T=0.005$, $\varepsilon_\uparrow = \varepsilon_\downarrow = -2$, and $W_{K,\sigma}^{(0)} = 100$. As before, the equilibrium Fermi energy defines the energy origin, and the nonequilibrium situation is characterized by $\mu_L = E_F + |\text{eV}|$ and $\mu_R = E_F$. In equilibrium, a Kondo peak at the Fermi energy is

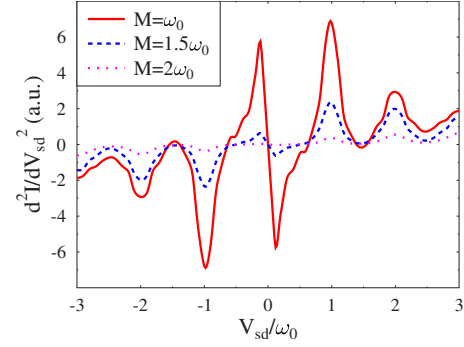


FIG. 5. (Color online) d^2I/dV_{sd}^2 for molecular junction in the Kondo regime. Shown are results for three choices of strength in coupling to vibration: $M=\Gamma/2$ (solid line), $M=2\Gamma/3$ (dashed line), and $M=\Gamma$ (dotted line). See text for other parameters.

seen. It splits into two (at each of the electrode Fermi energies) when finite bias is applied. Comparing to Figs. 1(a) and 1(b) of Ref. 32, we see that the present formalism essentially reproduces these results.

Inelastic effects are introduced into the picture as before, by dressing transfer-matrix elements by the shift operators, see Eqs. (14), (27), and (28). Figure 5 shows the result, obtained from such calculation for the second derivative of the current with respect to the source-drain voltage, for three choices of the electron-vibration coupling strength. Parameters of the calculation are (in units of $\Gamma_\sigma^{(0)}$) $T=0.025$, $\varepsilon_\sigma = -2$, $W_{K,\sigma}^{(0)} = 100$, and $\omega_0 = 0.5$. The solid, dashed, and dotted lines correspond to $M=0.5$, 0.75 , and 1 , respectively. As is expected, increase in electron-vibration interaction destroys the Kondo effect. The reasons for this are (a) dephasing due to electron-vibration interaction and (b) shift of the energy level due to phonon reorganization. Electronic level shift downward decreases the Kondo temperature ($T_K \sim \exp[-\pi|\varepsilon_\sigma|/\Gamma_\sigma]$, see Ref. 42), thus destroying the Kondo peak.

It should be emphasized that the vibrational structure seen in Fig. 5 is a normal inelastic tunneling feature that is seen to persist also in the Kondo regime. This feature appears both in the Kondo and normal blockade regimes [see Figs. 3(b) and 5], as indeed was recently observed in the molecular junction experiment of Yu *et al.*⁶ The transition between these regimes (when a molecular orbital crosses the Fermi energy) cannot be described by our approach for reasons outlined above. Also, Paaske and Flensberg⁴⁸ have recently applied a perturbative renormalization group to a limiting form of the same model in which the molecular electronic level is always in equilibrium with one side of the junction (the substrate in a scanning tunnelling microscopy configuration) and have shown that maintaining quantum coherence of vibrons, the effect disregarded in our treatment due to the approximation in Eq. (14), may lead to enhancement of the exchange coupling, and hence the Kondo temperature.

V. CONCLUSION

We study inelastic effects in electron transport through a model molecular junction in the Coulomb blockade and

Kondo regimes. The approach is based on nonequilibrium generalization of the equation-of-motion scheme introduced by Meir *et al.*^{10,31} and is appealingly simple. Inelastic effects are treated within a diabatic Born-Oppenheimer scheme. Important features of this approach are correct analytical results for both isolated molecule (no contacts) and noninteracting ($U=0$) cases, ability to reproduce results by Meir *et al.*³¹ without necessity of additional considerations to get the level population, no necessity for self-consistency to get exact (within the scheme) results when the electron-vibration interaction is switched off, and unified treatment of both Coulomb and (to some extent) Kondo at nonequilibrium. The approach is able to reproduce experimental features qualitatively.

Inelastic effects obtained within the model are resonant vibrational sidebands in the allowed part and IETS signal in the blockaded part of the conductance map in $V_g - V_{sd}$ coordinates, Franck-Condon blockade of transport for relatively strong electron-vibration interaction in the Coulomb blockade regime, and vibrational sidebands of the Kondo peak, as well as its quenching for strong vibronic coupling.

Generalization of these considerations to the case of a two-site molecular bridge in the junction is straightforward. The only problem is the large number of equations needed to be taken into account in this case. We postpone such generalization for future study.

ACKNOWLEDGMENTS

We are grateful to the MURI/DURINT program, to the NASA/URETI program, and to the NSF/MRSEC program for support of this research. A.N. thanks the Israel Science Foundation, the U.S.-Israel Binational Science Foundation, and the German-Israeli Foundation for financial support of this research.

APPENDIX A: DERIVATION OF EQUATION (21)

Here, we derive Eq. (21). Note that the derivation does not depend on whether V or \bar{V} (and similarly U or \bar{U}) is used for the system-lead coupling as long as the shift generator operator X is regarded as a scalar. We follow the procedure invented by Meir *et al.*^{10,30} for the equilibrium situation and generalize it to the Keldysh contour case, in order to take into account the nonequilibrium nature of molecular junction transport. During the derivation, we will treat transfer-matrix elements $\bar{V}_{k\sigma}$, Eq. (6), as numbers with the shift generator operators \hat{X}_σ , Eq. (7), incorporated into them as scalar parameters (a Born-Oppenheimer-type approximation). However, we will have to keep track of their dependence on time (or more precisely contour variable) in order to get the phonon correlation functions K correctly at the end.

We start from EOM for GF $G_\sigma^{(e)}(\tau, \tau')$, Eq. (15), on the Keldysh contour,

$$\begin{aligned} \left(i \frac{\partial}{\partial \tau} - \bar{\varepsilon}_\sigma \right) G_\sigma^{(e)}(\tau, \tau') &= \delta(\tau, \tau') + \bar{U} G_\sigma^{(2e)}(\tau, \tau') \\ &+ \sum_{k \in \{L, R\}} \bar{V}_{k\sigma}^\dagger(\tau) \Gamma_{k,\sigma}^{(1e)}(\tau, \tau'). \end{aligned} \quad (\text{A1})$$

New GFs on the right-hand side have the forms

$$\Gamma_{k,\sigma}^{(1e)}(\tau, \tau') = -i \langle T_c \hat{c}_{k\sigma}(\tau) \hat{d}_\sigma^\dagger(\tau') \rangle, \quad (\text{A2})$$

$$G_\sigma^{(2e)}(\tau, \tau') = -i \langle T_c \hat{d}_\sigma(\tau) \hat{n}_{\bar{\sigma}}(\tau) \hat{d}_\sigma^\dagger(\tau') \rangle. \quad (\text{A3})$$

Now we write EOMs for these GFs,

$$\left(i \frac{\partial}{\partial \tau} - \varepsilon_{k\sigma} \right) \Gamma_{k,\sigma}^{(1e)}(\tau, \tau') = \bar{V}_{k\sigma}(\tau) G_\sigma^{(e)}(\tau, \tau'), \quad (\text{A4})$$

$$\begin{aligned} \left(i \frac{\partial}{\partial \tau} - \bar{\varepsilon}_\sigma - \bar{U} \right) G_\sigma^{(2e)}(\tau, \tau') \\ = \delta(\tau, \tau') \langle \hat{n}_{\bar{\sigma}} \rangle + \sum_k [\bar{V}_{k\sigma}^\dagger(\tau) \Gamma_{1,k,\sigma}^{(2e)}(\tau, \tau') \\ + \bar{V}_{k\bar{\sigma}}(\tau) \Gamma_{2,k,\sigma}^{(2e)}(\tau, \tau') - \bar{V}_{k\bar{\sigma}}^\dagger(\tau) \Gamma_{3,k,\sigma}^{(2e)}(\tau, \tau')]. \end{aligned} \quad (\text{A5})$$

While the EOM in Eq. (A4) closes the chain of equations (its right-hand side contains only $G_\sigma^{(e)}$), the EOM for $G_\sigma^{(2e)}$ yields new correlations in its right-hand side defined by

$$\Gamma_{1,k,\sigma}^{(2e)}(\tau, \tau') = -i \langle T_c \hat{c}_{k\sigma}(\tau) \hat{n}_{\bar{\sigma}}(\tau) \hat{d}_\sigma^\dagger(\tau') \rangle, \quad (\text{A6})$$

$$\Gamma_{2,k,\sigma}^{(2e)}(\tau, \tau') = -i \langle T_c \hat{c}_{k\bar{\sigma}}^\dagger(\tau) \hat{d}_\sigma(\tau) \hat{d}_{\bar{\sigma}}(\tau) \hat{d}_\sigma^\dagger(\tau') \rangle, \quad (\text{A7})$$

$$\Gamma_{3,k,\sigma}^{(2e)}(\tau, \tau') = -i \langle T_c \hat{c}_{k\bar{\sigma}}(\tau) \hat{d}_{\bar{\sigma}}^\dagger(\tau) \hat{d}_\sigma(\tau) \hat{d}_\sigma^\dagger(\tau') \rangle. \quad (\text{A8})$$

As a last step in the chain of EOMs, we follow Refs. 10 and 30 by writing equations for the GFs, in Eqs. (A6)–(A8),

$$\begin{aligned} \left(i \frac{\partial}{\partial \tau} - \varepsilon_{k\sigma} \right) \Gamma_{1,k,\sigma}^{(2e)}(\tau, \tau') \\ = \bar{V}_{k\sigma}(\tau) G_\sigma^{(2e)}(\tau, \tau') + \sum_{k'} [\bar{V}_{k'\bar{\sigma}}(\tau) \Gamma_{1,k',\sigma}^{(3e)}(\tau, \tau') \\ - \bar{V}_{k'\bar{\sigma}}^\dagger(\tau) \Gamma_{2,k',\sigma}^{(3e)}(\tau, \tau')], \end{aligned} \quad (\text{A9})$$

$$\begin{aligned} \left(i \frac{\partial}{\partial \tau} + \varepsilon_{k\bar{\sigma}} - \bar{\varepsilon}_\sigma - \bar{\varepsilon}_{\bar{\sigma}} - \bar{U} \right) \Gamma_{2,k,\sigma}^{(2e)}(\tau, \tau') \\ = \bar{V}_{k\bar{\sigma}}^\dagger(\tau) G_\sigma^{(2e)}(\tau, \tau') - \sum_{k'} [\bar{V}_{k'\sigma}^\dagger(\tau) \Gamma_{3,k',\sigma}^{(3e)}(\tau, \tau') \\ + \bar{V}_{k'\bar{\sigma}}^\dagger(\tau) \Gamma_{4,k',\sigma}^{(3e)}(\tau, \tau')], \end{aligned} \quad (\text{A10})$$

$$\begin{aligned} \left(i \frac{\partial}{\partial \tau} - \varepsilon_{k\bar{\sigma}} - \bar{\varepsilon}_\sigma + \bar{\varepsilon}_{\bar{\sigma}} \right) \Gamma_{3,k,\sigma}^{(2e)}(\tau, \tau') \\ = \bar{V}_{k\bar{\sigma}}(\tau) [G_\sigma^{(e)}(\tau, \tau') - G_\sigma^{(2e)}(\tau, \tau')] - \sum_{k'} [\bar{V}_{k'\bar{\sigma}}(\tau) \\ \times \Gamma_{5,k',\sigma}^{(3e)}(\tau, \tau') - \bar{V}_{k'\sigma}^\dagger(\tau) \Gamma_{6,k',\sigma}^{(3e)}(\tau, \tau')]. \end{aligned} \quad (\text{A11})$$

On the right-hand side of these equations, we now have new, higher-order GFs, $\Gamma_{j,k',\sigma}^{(3e)}$ defined by the middle terms of Eqs. (A12)–(A17). GFs $\Gamma^{(2e)}$ and $\Gamma^{(3e)}$ take account of spin corre-

lations in the leads. Closure of the (in principle infinite) EOM chain is achieved assuming that higher-order spin correlations in the leads can be neglected. Thus, following Ref. 10, the terms $\Gamma^{(3e)}$ are expressed in terms of lower-order GFs,

$$\Gamma_{1,k',k,\sigma}^{(3e)}(\tau, \tau') = -i \langle T_c \hat{c}_{k'\bar{\sigma}}^\dagger(\tau) \hat{c}_{k\sigma}(\tau) \hat{d}_{\bar{\sigma}}^\dagger(\tau) \hat{d}_{\sigma}^\dagger(\tau') \rangle \approx 0, \quad (\text{A12})$$

$$\Gamma_{2,k',k,\sigma}^{(3e)}(\tau, \tau') = -i \langle T_c \hat{c}_{k\sigma}(\tau) \hat{c}_{k'\bar{\sigma}}^\dagger(\tau) \hat{d}_{\bar{\sigma}}^\dagger(\tau) \hat{d}_{\sigma}^\dagger(\tau') \rangle \approx 0, \quad (\text{A13})$$

$$\Gamma_{3,k',k,\sigma}^{(3e)}(\tau, \tau') = -i \langle T_c \hat{c}_{k'\sigma}(\tau) \hat{c}_{k\bar{\sigma}}^\dagger(\tau) \hat{d}_{\bar{\sigma}}^\dagger(\tau) \hat{d}_{\sigma}^\dagger(\tau') \rangle \approx 0, \quad (\text{A14})$$

$$\begin{aligned} \Gamma_{4,k',k,\sigma}^{(3e)}(\tau, \tau') &= -i \langle T_c \hat{c}_{k\bar{\sigma}}^\dagger(\tau) \hat{c}_{k'\sigma}(\tau) \hat{d}_{\sigma}(\tau) \hat{d}_{\sigma}^\dagger(\tau') \rangle \\ &\approx \delta_{k,k'} \langle \hat{n}_{k\bar{\sigma}} \rangle G_{\sigma}^{(e)}(\tau, \tau'), \end{aligned} \quad (\text{A15})$$

$$\begin{aligned} \Gamma_{5,k',k,\sigma}^{(3e)}(\tau, \tau') &= -i \langle T_c \hat{c}_{k\bar{\sigma}}(\tau) \hat{c}_{k'\sigma}^\dagger(\tau) \hat{d}_{\sigma}(\tau) \hat{d}_{\sigma}^\dagger(\tau') \rangle \\ &\approx \delta_{k,k'} [1 - \langle \hat{n}_{k\bar{\sigma}} \rangle] G_{\sigma}^{(e)}(\tau, \tau'), \end{aligned} \quad (\text{A16})$$

$$\Gamma_{6,k',k,\sigma}^{(3e)}(\tau, \tau') = -i \langle T_c \hat{c}_{k\bar{\sigma}}(\tau) \hat{d}_{\bar{\sigma}}^\dagger(\tau) \hat{c}_{k'\sigma}(\tau) \hat{d}_{\sigma}^\dagger(\tau') \rangle \approx 0. \quad (\text{A17})$$

Now, using Eqs. (A12)–(A17) in Eqs. (A9)–(A11), one can solve for $\Gamma_{i,k,\sigma}^{(2e)}$ ($i=\{1,2,3\}$) in terms of $G_{\sigma}^{(e)}$ and $G_{\sigma}^{(2e)}$,

$$\Gamma_{1,k,\sigma}^{(2e)} = g_{k,\sigma} \bar{V}_{k\sigma} \circ G_{\sigma}^{(2e)}, \quad (\text{A18})$$

$$\Gamma_{2,k,\sigma}^{(2e)} = g_{k,\bar{\sigma}} \bar{V}_{k\bar{\sigma}}^\dagger \circ (G_{\sigma}^{(2e)} - \langle \hat{n}_{k\bar{\sigma}} \rangle G_{\sigma}^{(e)}), \quad (\text{A19})$$

$$\Gamma_{3,k,\sigma}^{(2e)} = g_{k,\bar{\sigma}} \bar{V}_{k\bar{\sigma}} \circ (\langle \hat{n}_{k\bar{\sigma}} \rangle G_{\sigma}^{(e)} - G_{\sigma}^{(2e)}), \quad (\text{A20})$$

where we have used the short notation style with “ \circ ” implying convolution of two functions on the contour ($A \circ B$)(τ, τ') = $\int_c d\tau'' A(\tau, \tau'') B(\tau'', \tau')$. These solutions are substituted into Eq. (A5) which gives $G_{\sigma}^{(2e)}$ in terms of $G_{\sigma}^{(e)}$. Finally, the last result, together with Eq. (A4), can be used in Eq. (A1) to get an equation for $G_{\sigma}^{(e)}$ in the form

$$G_{\sigma}^{(e)} = G_{2,\sigma}^{(e)} + U \langle \hat{n}_{\bar{\sigma}} \rangle G_{2,\sigma}^{(e)} \circ G_{1,\sigma}^{(e)}. \quad (\text{A21})$$

$G_{i,\sigma}^{(e)}$ ($i=\{1,2,3,4\}$) are defined in Eqs. (22)–(26) while self-energies entering these definitions are given by Eqs. (27)–(30).

In order to simplify the structure, we rewrite it in the form

$$G_{\sigma}^{(e)} = (1 - \langle \hat{n}_{\bar{\sigma}} \rangle) G_{2,\sigma}^{(e)} + \langle \hat{n}_{\bar{\sigma}} \rangle \{ G_{2,\sigma}^{(e)} + U G_{2,\sigma}^{(e)} \circ G_{1,\sigma}^{(e)} \} \quad (\text{A22})$$

and note that

$$\{\dots\} = G_{2,\sigma}^{(e)} \circ G_{1,\sigma}^{(e)} (\hat{G}_{1,\sigma}^{-1} + U) = G_{2,\sigma}^{(e)} \circ G_{1,\sigma}^{(e)} \hat{G}_{4,\sigma}^{-1} = G_{3,\sigma}^{(e)}. \quad (\text{A23})$$

The last equation follows from $\hat{G}_{1,\sigma}^{-1} \hat{G}_{2,\sigma}^{-1} = \hat{G}_{4,\sigma}^{-1} \hat{G}_{3,\sigma}^{-1}$. Substitution of Eq. (A23) into Eq. (A22) leads to Eq. (21). The retarded projection of Eq. (21) is the final result of Ref. 10.

APPENDIX B: ANALYTICAL EXPRESSION FOR SELF-ENERGY $\Sigma_{\sigma 1}^{(\infty)}$

Here, we derive analytical expressions for retarded and lesser projections of $\Sigma_{\sigma 1}^{(\infty)}$, Eq. (54), under Lorentzian assumption for coupling between molecule and contacts, Eq. (44). In the case of a dense continuum of states in the contacts (assumed here), the sum in Eq. (54) can be converted to an integral, then, retarded and lesser projections of the SE (in energy domain) are

$$\Sigma_{\sigma 1}^{(\infty)r}(E) = \sum_{K=L,R} \int_{-\infty}^{+\infty} \frac{d\epsilon}{2\pi} \frac{\Gamma_{K,\bar{\sigma}}(\epsilon) f_K(\epsilon)}{E - \epsilon - \epsilon_{\sigma} + \epsilon_{\bar{\sigma}} + i\gamma_{\sigma}/2}, \quad (\text{B1})$$

$$\begin{aligned} \Sigma_{\sigma 1}^{(\infty)<}(E) &= i \sum_{K=L,R} \int_{-\infty}^{+\infty} \frac{d\epsilon}{2\pi} \frac{\Gamma_{K,\bar{\sigma}}(\epsilon) f_K^2(\epsilon)}{(E - \epsilon - \epsilon_{\sigma} + \epsilon_{\bar{\sigma}})^2 + (\gamma_{\sigma}/2)^2} \\ &\approx i \sum_{K=L,R} \int_{-\infty}^{+\infty} \frac{d\epsilon}{2\pi} \frac{\Gamma_{K,\bar{\sigma}}(\epsilon) f_K(\epsilon)}{(E - \epsilon - \epsilon_{\sigma} + \epsilon_{\bar{\sigma}})^2 + (\gamma_{\sigma}/2)^2}, \end{aligned} \quad (\text{B2})$$

where the second line of Eq. (B2) is correct for the case of $T \rightarrow 0$ (relevant for observation of the Kondo peak).

Introducing

$$x = \beta(\epsilon - \mu_K), \quad (\text{B3})$$

we arrive at integrals of the forms

$$\int_{-\infty}^{+\infty} dx \frac{1}{(x-x_1)(x-x_2)(x-x_3)} \frac{1}{e^x + 1}, \quad (\text{B4})$$

$$\int_{-\infty}^{+\infty} dx \frac{1}{(x-x_1)(x-x_2)(x-x_3)(x-x_4)} \frac{1}{e^x + 1} \quad (\text{B5})$$

for Eqs. (B1) and (B2), respectively, where

$$x_1 = \beta(E_{K,\bar{\sigma}}^{(0)} - \mu_K + iW_{K,\bar{\sigma}}^{(0)}), \quad (\text{B6})$$

$$x_2 = x_1^*, \quad (\text{B7})$$

$$x_3 = \beta\left(E - \epsilon_{\sigma} + \epsilon_{\bar{\sigma}} - \mu_K + i\frac{\gamma_{\sigma}}{2}\right), \quad (\text{B8})$$

$$x_4 = x_3^*, \quad (\text{B9})$$

with $K=L,R$. These integrals can be taken analytically by complex contour integration; the poles are at x_1, x_2, x_3 [x_4 in the case of the integral in Eq. (B5)] and also at $y_n \equiv i\pi(2n+1)$; $n=0, \pm 1, \pm 2, \dots$. Performing the integration, one arrives at the following expressions for the SE projections:

$$\Sigma_{\sigma 1}^{(\infty)r}(E) = \sum_{K=L,R} \left\{ \frac{i\Gamma_{K,\bar{\sigma}}^{(0)} W_{K,\bar{\sigma}}^{(0)}}{4\pi} \left[\frac{\psi^*\left(\frac{\pi - ix_1}{2\pi}\right)}{E_2 + i(W_{K,\bar{\sigma}}^{(0)} + \gamma_{\bar{\sigma}}/2)} - \frac{\psi\left(\frac{\pi - ix_1}{2\pi}\right)}{E_2 - i(W_{K,\bar{\sigma}}^{(0)} - \gamma_{\bar{\sigma}}/2)} \right] - \frac{\Gamma_{K,\bar{\sigma}}^{(0)} (W_{K,\bar{\sigma}}^{(0)})^2}{2\pi} \frac{\psi\left(\frac{\pi - ix_3}{2\pi}\right)}{[E_2 - i(W_{k,\bar{\sigma}}^{(0)} - \gamma_{\bar{\sigma}}/2)][E_2 + i(W_{k,\bar{\sigma}}^{(0)} + \gamma_{\bar{\sigma}}/2)]} + \frac{\Gamma_{k,\bar{\sigma}}^{(0)} W_{k,\bar{\sigma}}^{(0)}}{4} \frac{1}{E_2 + i(W_{k,\bar{\sigma}}^{(0)} + \gamma_{\bar{\sigma}}/2)} \right\}, \quad (\text{B10})$$

$$\Sigma_{\sigma 1}^{(\infty)<}(E) = i \sum_{K=L,R} \Gamma_{k,\bar{\sigma}}^{(0)} \left(\frac{W_{k,\bar{\sigma}}^{(0)} \gamma_{\bar{\sigma}}}{2\pi} \text{Im} \left\{ \frac{\psi\left(\frac{\pi - ix_1}{2\pi}\right)}{[E_2 - i(W_{k,\bar{\sigma}}^{(0)} - \gamma_{\bar{\sigma}}/2)][E_2 - i(W_{k,\bar{\sigma}}^{(0)} + \gamma_{\bar{\sigma}}/2)]} \right\} + \frac{(W_{k,\bar{\sigma}}^{(0)})^2}{\pi} \text{Im} \left\{ \frac{\psi\left(\frac{\pi - ix_3}{2\pi}\right)}{[E_2 - i(W_{k,\bar{\sigma}}^{(0)} - \gamma_{\bar{\sigma}}/2)][E_2 + i(W_{k,\bar{\sigma}}^{(0)} + \gamma_{\bar{\sigma}}/2)]} \right\} + \frac{W_{k,\bar{\sigma}}^{(0)}}{2} \left(W_{k,\bar{\sigma}}^{(0)} + \frac{\gamma_{\bar{\sigma}}}{2} \right) \frac{1}{E_2^2 + (W_{k,\bar{\sigma}}^{(0)} + \gamma_{\bar{\sigma}}/2)^2} \right), \quad (\text{B11})$$

with $E_2 = E - \varepsilon_{\sigma} + \varepsilon_{\bar{\sigma}} - E_{k,\bar{\sigma}}^{(0)}$ and where ψ is a psi (digamma) function.⁴⁹ Note that it is the second term in Eq. (B10) which is responsible for the Kondo effect appearance.

-
- ¹M. A. Reed, C. Zhou, C. J. Muller, T. P. Burgin, and J. M. Tour, *Science* **278**, 252 (1997).
- ²J. Park, A. N. Pasupathy, J. I. Goldsmith, C. Chang, Y. Yaish, J. R. Petta, M. Rinkoski, J. P. Sethna, H. D. Abruña, P. L. McEuen, and D. C. Ralph, *Nature (London)* **417**, 722 (2002); J. Park, A. N. Pasupathy, J. I. Goldsmith, A. V. Soldatov, C. Chang, Y. Yaish, J. P. Sethna, H. D. Abruña, D. C. Ralph, and P. L. McEuen, *Thin Solid Films* **438-439**, 457 (2003).
- ³W. Liang, M. P. Shores, M. Bockrath, J. R. Long, and H. Park, *Nature (London)* **417**, 725 (2002).
- ⁴N. B. Zhitenev, H. Meng, and Z. Bao, *Phys. Rev. Lett.* **88**, 226801 (2002).
- ⁵S. Kubatkin, A. Danilov, M. Hjort, J. Cornil, J.-L. Brédas, N. Stuhr-Hansen, P. Hedergård, and T. Bjørnholm, *Nature (London)* **425**, 698 (2003).
- ⁶L. H. Yu and D. Natelson, *Nano Lett.* **4**, 79 (2004); L. H. Yu, Z. K. Keane, J. W. Ciszek, L. Cheng, M. P. Stewart, J. M. Tour, and D. Natelson, *Phys. Rev. Lett.* **93**, 266802 (2004).
- ⁷M. Poot, E. Osorio, K. O'Neil, J. M. Thijssen, D. Vanmaekelbergh, C. A. van Walree, L. W. Jenneskens, and H. S. J. van der Zant, *Nano Lett.* **6**, 1031 (2006).
- ⁸H. Park, J. Park, A. Lim, E. Anderson, A. Alivisatos, and P. McEuen, *Nature (London)* **407**, 57 (2000).
- ⁹C. W. J. Beenakker, *Phys. Rev. B* **44**, 1646 (1991).
- ¹⁰Y. Meir, N. S. Wingreen, and P. A. Lee, *Phys. Rev. Lett.* **66**, 3048 (1991).
- ¹¹L. Craco and K. Kang, *Phys. Rev. B* **59**, 12244 (1999).
- ¹²P. S. Cornaglia, H. Ness, and D. R. Grempel, *Phys. Rev. Lett.* **93**, 147201 (2004); P. S. Cornaglia, D. R. Grempel, and H. Ness, *Phys. Rev. B* **71**, 075320 (2005).
- ¹³L. Arrachea and M. J. Rozenberg, *Phys. Rev. B* **72**, 041301(R) (2005).
- ¹⁴S. A. Gurvitz, D. Mozyrsky, and G. P. Berman, *Phys. Rev. B* **72**, 205341 (2005); **72**, 249902(E) (2005).
- ¹⁵B. Muralidharan, A. W. Ghosh, and S. Datta, *Phys. Rev. B* **73**, 155410 (2006).
- ¹⁶D. C. Langreth and P. Nordlander, *Phys. Rev. B* **43**, 2541 (1991); H. Shao, D. C. Langreth, and P. Nordlander, *ibid.* **49**, 13929 (1994); P. Nordlander, N. S. Wingreen, Y. Meir, and D. C. Langreth, *ibid.* **61**, 2146 (2000).
- ¹⁷N. S. Wingreen and Y. Meir, *Phys. Rev. B* **49**, 11040 (1994).
- ¹⁸M. Krawiec and K. I. Wysokiński, *Phys. Rev. B* **66**, 165408 (2002).
- ¹⁹A. D. Güçlü, Q.-F. Sun, and H. Guo, *Phys. Rev. B* **68**, 245323 (2003).
- ²⁰T.-K. Ng, *Phys. Rev. Lett.* **76**, 487 (1996).
- ²¹Q.-F. Sun and T.-H. Lin, *J. Phys.: Condens. Matter* **9**, 4875 (1997); C. Niu, D. L. Lin, and T.-H. Lin, *ibid.* **11**, 1511 (1999); M. Krawiec and K. I. Wysokiński, *Phys. Rev. B* **73**, 075307 (2006).
- ²²R. Świrkwicz, J. Barnaś, and M. Wilczyński, *Phys. Rev. B* **68**, 195318 (2003); R. Świrkwicz, M. Wilczyński, and J. Barnaś, *J. Phys.: Condens. Matter* **18**, 2291 (2006).
- ²³A. L. Yeyati, A. Martín-Rodero, and F. Flores, *Phys. Rev. Lett.* **71**, 2991 (1993).
- ²⁴A. Rosch, J. Paaske, J. Kroha, and P. Wölfle, *Phys. Rev. Lett.* **90**, 076804 (2003); *J. Phys. Soc. Jpn.* **74**, 118 (2005); J. Paaske, A. Rosch, and P. Wölfle, *Phys. Rev. B* **69**, 155330 (2004).
- ²⁵A. Kaminski, Yu. V. Nazarov, and L. I. Glazman, *Phys. Rev. Lett.* **83**, 384 (1999); *Phys. Rev. B* **62**, 8154 (2000).
- ²⁶T. Fujii and K. Ueda, *Phys. Rev. B* **68**, 155310 (2003); *Physica E (Amsterdam)* **22**, 498 (2004).
- ²⁷A. Komnik and A. O. Gogolin, *Phys. Rev. B* **69**, 153102 (2004).
- ²⁸J. König, H. Schoeller, and G. Schön, *Phys. Rev. B* **58**, 7882 (1998).
- ²⁹M. Hamasaki, *Phys. Rev. B* **69**, 115313 (2004); arXiv:cond-mat/0408416 (unpublished).
- ³⁰H. Haug and A.-P. Jauho, *Quantum Kinetics in Transport and*

- Optics of Semiconductors* (Springer, Berlin, 1996).
- ³¹Y. Meir, N. S. Wingreen, and P. A. Lee, Phys. Rev. Lett. **70**, 2601 (1993).
- ³²R. A. Marcus, J. Chem. Phys. **24**, 966 (1956); **24** 979 (1956).
- ³³G. D. Mahan, *Many-Particle Physics*, 3rd ed. (Kluwer Academic, Dordrecht/Plenum, New York, 2000).
- ³⁴M. Galperin, A. Nitzan, and M. A. Ratner, Phys. Rev. B **73**, 045314 (2006).
- ³⁵Y. Meir and N. S. Wingreen, Phys. Rev. Lett. **68**, 2512 (1992); A. P. Jauho, N. S. Wingreen, and Y. Meir, Phys. Rev. B **50**, 5528 (1994).
- ³⁶Note that the diagrammatic technique becomes unusable also due to the presence of shift operators \hat{X} in the transfer-matrix elements. Their many-body character makes Wick's theorem inapplicable.
- ³⁷D. Natelson, in *Handbook of Organic Electronics and Photonics*, edited by H. S. Nalwa (American Scientific, Stevenson Ranch, CA, 2006).
- ³⁸In a zero-order calculation, no iterations are employed to attain convergence of electron-phonon coupling effect. This amounts to assuming that the phonon remains at its original thermal equilibrium even when coupled to the nonequilibrium electronic system.
- ³⁹A. Mitra, I. Aleiner, and A. J. Millis, Phys. Rev. B **69**, 245302 (2004).
- ⁴⁰J. Koch and F. von Oppen, Phys. Rev. Lett. **94**, 206804 (2005).
- ⁴¹A. W. Ghosh, T. Rakshit, and S. Datta, Nano Lett. **4**, 565 (2004).
- ⁴²A. C. Hewson, *The Kondo Problem to Heavy Fermions* (Cambridge University Press, Cambridge, 1993).
- ⁴³R. Aguado and D. C. Langreth, Phys. Rev. Lett. **85**, 1946 (2000).
- ⁴⁴K. Kang, S. Y. Cho, J.-J. Kim, and S.-C. Shin, Phys. Rev. B **63**, 113304 (2001).
- ⁴⁵Note, however, recent publications (Refs. 46 and 47) where the possibility of observing a Kondo effect at finite bias for the spin-singlet ground state was reported.
- ⁴⁶M. N. Kiselev, K. Kikoin, and L. W. Molenkamp, Phys. Rev. B **68**, 155323 (2003).
- ⁴⁷J. Paaske, A. Rosch, P. Wölfle, N. Mason, C. M. Marcus, and J. Nygård, Nature (London) **2**, 460 (2006).
- ⁴⁸J. Paaske and K. Flensberg, Phys. Rev. Lett. **94**, 176801 (2005).
- ⁴⁹M. Abramowitz and I. A. Stegun, *Handbook of Mathematical Functions with Formulas, Graphs, and Mathematical Tables*, 10th ed. (U. S. Department of Commerce, Washington, DC, 1972).